



## Original article

## Anticancer effects of the metabolic products of the resveratrol analogue, DMU-212: Structural requirements for potency

Vasilis P. Androustopoulos<sup>a,d,\*</sup>, Ketan C. Ruparelia<sup>b</sup>, Athanasios Papakyriakou<sup>c</sup>, Harilaos Filippakis<sup>a</sup>, Aristeidis M. Tsatsakis<sup>d</sup>, Demetrios A. Spandidos<sup>a</sup>

<sup>a</sup>Laboratory of Clinical Virology, University of Crete, Medical School, Voutes, 71003 Heraklion, Crete, Greece

<sup>b</sup>De Montfort University, Leicester School of Pharmacy, Leicester LE1 9BH, UK

<sup>c</sup>Laboratory of Chemical Biology of Natural Products and Designed Molecules, Institute of Physical Chemistry, NSRF Demokritos, 15310 Agia Paraskevi, Athens, Greece

<sup>d</sup>Laboratory of Toxicology, University of Crete, Medical School, Voutes, 71003 Heraklion, Crete, Greece

## ARTICLE INFO

## Article history:

Received 15 November 2010

Received in revised form

17 March 2011

Accepted 22 March 2011

Available online 30 March 2011

## Keywords:

Resveratrol

DMU-212

MCF-7 cells

HepG2 cells

Antiproliferation

Apoptosis

Cell cycle inhibition

β-Tubulin

Paclitaxel binding site

Molecular modeling

Docking

## ABSTRACT

The methoxylated *trans*-stilbene resveratrol analogue, (E)-3,4,5,4'-tetramethoxystilbene (**1**), has shown promising antiproliferative activity in *in vitro* cell line and *in vivo* models. *In vivo* **1** gives rise to several metabolic products through demethylation or hydroxylation reactions at the stilbene moiety. In the present study we examined the anticancer activity of **1** and the metabolites (E)-3'-hydroxy-3,4,5,4'-tetramethoxystilbene (**2**), (E)-4'-hydroxy-3,4,5-trimethoxystilbene (**3**), (E)-4-hydroxy-3,5,4'-trimethoxystilbene (**4**) and (E)-3-hydroxy-4,5,4'-trimethoxystilbene (**5**) by means of cell viability testing, cell cycle analysis, immunostaining and Western blotting. Compounds **1** and **2** exhibited submicromolar toxicity in MCF-7 breast adenocarcinoma and HepG2 hepatoma cells, whereas **3**, **4** and **5** were inactive in terms of inhibition of cellular proliferation. Incubation with **1** or **2** at 10 μM for 24 h induced apoptosis and G2/M cell cycle arrest in MCF-7 and HepG2 cells. Immunostaining of MCF-7 cells for β-tubulin in the presence of either **1** or **2** revealed shorter localization of the protein around the nucleus, as compared to control cells. Western blot analyses further demonstrated that treatment with either **1** or **2** at concentrations between 30 and 50 μM for 24 h caused a downregulation in the levels of β-tubulin and cyclin D1 expression and an upregulation in the levels of p53 expression in MCF-7 and HepG2 cells. **2** further increased the ratio of mRNA levels of the apoptosis-related genes Bax/Bcl-xL in both MCF-7 and HepG2 cells in a dose-dependent manner. We conclude that **2** inhibits HepG2 and MCF-7 cellular proliferation by inducing apoptosis and G2/M arrest through p53 and Bax/Bcl-xL upregulation. Our findings further demonstrate that trimethoxy substitutions along with the presence of a methoxy group at position 4' are necessary for retaining the activity of **1**.

© 2011 Elsevier Masson SAS. All rights reserved.

## 1. Introduction

Resveratrol is a naturally occurring phytoalexin, which is produced in plants in response to stress and environmental

pathogenic attack. It is concentrated in high amounts in the skin of grapes, cranberries, peanuts and other dietary constituents and has been the focus of extensive investigation due to its chemopreventive effect in *in vitro* and *in vivo* models. Resveratrol possesses a wide spectrum of anticancer activities. *In vitro* it was found to inhibit the formation of preneoplastic lesions in a 7,12-dimethylbenz(a)anthracene (DMBA)-induced mouse mammary organ culture [1], as well as the TCDD-mediated induction of CYP1A1 mRNA and CYP1A1 activity in human hepatoma cells by preventing the binding of the AhR to the CYP1A1 promoter [2]. Furthermore, resveratrol affects the cell cycle of cancer cells as it inhibits the activities of protein kinase C and D [3,4]. It also induces apoptosis [5] and decreases the activity of the transcription factors NFκB and AP-1 [6,7]. In animal studies, resveratrol was found to interfere with the formation of azoxymethane-induced aberrant

**Abbreviations:** DMU-212, (E)-3,4,5,4'-tetramethoxystilbene; DMU-214, (E)-3'-hydroxy-3,4,5,4'-tetramethoxystilbene; DMU-281, (E)-4'-hydroxy-3,4,5-trimethoxystilbene; DMU-291, (E)-4-hydroxy-3,5,4'-trimethoxystilbene; DMU-807, (E)-3-hydroxy-4,5,4'-trimethoxystilbene; MTT, 3-(4,5-dimethylthiazole-2-yl)-2,5-diphenyl tetrazolium bromide; DTT, DL-dithiothreitol; FACS, fluorescence-activated cell sorting; p53, protein 53.

\* Corresponding author. Laboratory of Toxicology, University of Crete, Medical School, Voutes, 71003 Heraklion, Crete, Greece. Tel.: +30 2810 394870; fax: +30 2810 542098.

E-mail addresses: [vandrou@med.uoc.gr](mailto:vandrou@med.uoc.gr), [vasilis\\_androustopoulos@yahoo.com](mailto:vasilis_androustopoulos@yahoo.com) (V.P. Androustopoulos).

cryptic foci in rat colon and decrease adenoma development in the small intestine of Apc<sup>Min+</sup> mice [8,9].

Although the anticancer activities of resveratrol are apparent, the efficacy of this natural compound is limited because of its poor bioavailability. As in the case of polyhydroxylated flavonoids, the chemical structure of resveratrol, which contains three free hydroxyl groups, renders it susceptible to extensive phase-II conjugation reactions *in vivo*. One study in humans demonstrated the potential drawbacks of the poor bioavailability of resveratrol [10]. To improve the pharmacokinetic properties of resveratrol and extend its cancer-protecting activity, several synthetic analogues have been generated and tested in *in vitro* models. One promising strategy involves the introduction of methoxy substitutions in place of the hydroxyl groups of the stilbene structure. Synthesis of methoxylated analogues of resveratrol has been an active area of research for the design of novel chemotherapeutic drugs with improved pharmacological activities. Numerous studies have supported the conclusion that introduction of methoxy substitutions in place of hydroxyl groups in the structure of resveratrol improves the antiproliferative effect of the latter by means of induction of apoptosis and cell cycle inhibition [5,11].

The fully methylated analogue of resveratrol, (E)-3,5,4'-trimethoxystilbene, has been documented to possess strong antiangiogenic and antivasular activity [12]. Similarly, the stilbenoid analogue of resveratrol, (E)-3,4,5,4'-tetramethoxystilbene or DMU-212 (**1**), possesses enhanced anticancer activity in terms of the induction of apoptosis and antiproliferation compared to resveratrol [5]. In addition, **1** showed improved bioavailability in mouse liver and plasma compared to resveratrol [13]. **1** escapes glucuronidation reactions due to its methoxy groups and is metabolized *in vivo* to four major metabolites (E)-3'-hydroxy-3,4,5,4'-tetramethoxystilbene or DMU-214 (**2**), (E)-4'-hydroxy-3,4,5-trimethoxystilbene or DMU-281 (**3**), (E)-4-hydroxy-3,5,4'-trimethoxystilbene or DMU-291 (**4**), and (E)-3-hydroxy-4,5,4'-trimethoxystilbene or DMU-807 (**5**) [13]. However, whether these metabolites retain the biological activity of **1** remains unknown.

In order to elucidate the cancer therapeutic potential of **1**, we compared the biological activities of the latter with that of its metabolites in cancer cell lines. The structures of resveratrol, **1** and metabolites are shown in Fig. 1. In addition, our study aimed to identify the structural components of **1** in regards to its metabolic products, which are required for the antiproliferative activity of this anticancer agent.

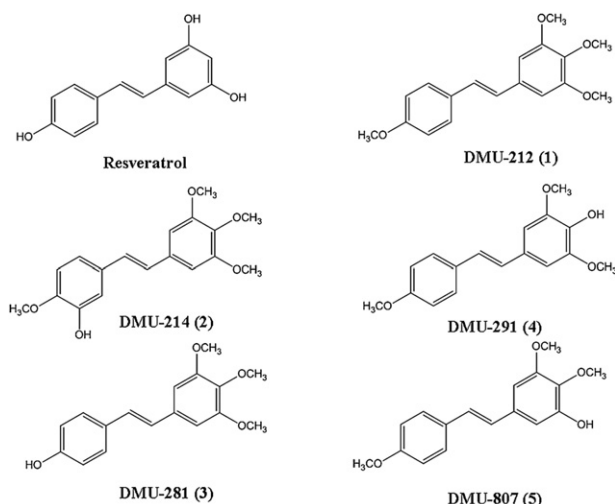


Fig. 1. Chemical structures of resveratrol and the synthetic analogues **1**, **2**, **3**, **4** and **5**.

## 2. Results

### 2.1. NMR and mass spectrometric characterization

#### 2.1.1. (E)-3,4,5,4'-Tetramethoxystilbene (**1**)

White crystals (0.20 g, 28%), m.p. 152–153 °C; *m/z* [FAB] 301 ( $[M + 1]^+$ , 100%),  $\delta_H$  (CDCl<sub>3</sub>) 3.80 (3H, s, OMe) 3.85 (3H, s, OMe), 3.90 (6H, s, 2 × OMe), 6.75 (2H, s, ArH), 6.93 (1H, d, *J* = 16.6 Hz, C=CH), 6.95 (2H, m, ArH), 7.00 (1H, d, *J* = 16.6 Hz, C=CH), 7.48 (2H, d, ArH).  $\delta_C$  (CDCl<sub>3</sub>), 55.35, 56.19, 60.97, 103.53, 114.22, 126.65, 127.67, 127.81, 130.10, 133.48, 137.86, 153.47, 159.39; Anal. Calcd C<sub>18</sub>H<sub>20</sub>O<sub>4</sub>: C, 71.98; H, 6.71. Found C, 71.66; H, 6.75. HRMS found  $[M + H]^+$  301.1434, C<sub>18</sub>H<sub>21</sub>O<sub>4</sub> requires  $[M + H]^+$  301.1434.

#### 2.1.2. 3-Tert-butyltrimethylsilyloxy-4-methoxybenzaldehyde precursor of **2**

Colourless oil (8.54 g 98%); *m/z* [FAB] 267 ( $[M]^+$ , 100%);  $\delta_H$  (CDCl<sub>3</sub>) 0.30 (6H, s, Si(CH<sub>3</sub>)<sub>2</sub>), 0.9 (9H, s, C(CH<sub>3</sub>)<sub>3</sub>), 3.80 (3H, s, OMe), 6.95 (1H, d, ArH), 7.35 (1H, d, ArH), 7.45 (H, dd, ArH), 9.00 (1H, s, CHO);  $\delta_C$  (CDCl<sub>3</sub>), 18.80, 26.02, 55.86, 55.95, 111.38, 111.62, 120.50, 122.74, 125.38, 126.55, 130.67, 191.22.

#### 2.1.3. (E)-3'-Hydroxy-3,4,5,4'-tetramethoxystilbene (**2**)

White solid (0.50 g 73%); TLC: *R<sub>f</sub>* 0.55 (ethyl acetate/petroleum ether 4:6); *m/z* [FAB] 317 ( $[M + 1]^+$ , 100%),  $\delta_H$  (CDCl<sub>3</sub>) 3.90 (3H, s, OMe), 3.85 (9H, s, 3 × OMe), 5.70 (1H, bs, OH), 6.7 (2H, s, ArH), 6.80 (1H, d, *J* = 15 Hz, CH=CH), 6.90 (2H, d, *J* = 15 Hz, CH=CH), 6.95 (1H, d, ArH), 7.10 (1H, d, ArH).  $\delta_C$  (CDCl<sub>3</sub>), 53.24, 56.15, 60.49, 61.01, 103.37, 110.73, 111.80, 119.28, 127.06, 130.99, 133.40, 137.67, 145.85, 152.89; HRMS found  $[M + 1]^+$  317.1386, C<sub>18</sub>H<sub>21</sub>O<sub>5</sub> requires  $[M + 1]^+$  317.1384.

#### 2.1.4. (E)-3'-Hydroxy-3,4,5,4'-tetramethoxystilbene (**3**)

White solid (0.10 g, 62%), m.p. 152–154 °C; TLC: *R<sub>f</sub>* 0.30 (ethyl acetate/petroleum ether 2:8); *m/z* [FAB] 286 ( $[M + 1]^+$ , 75%),  $\delta_H$  (CDCl<sub>3</sub>) 3.80 (3H, s, OMe), 3.90 (6H, s, 2 × OMe), 5.00 (1H, bs, OH), 6.70 (2H, s, ArH), 6.82 (2H, d, ArH), 6.85 (1H, d, *J* = 16 Hz, CH=CH), 6.95 (1H, d, *J* = 16 Hz, CH=CH), 7.39 (2H, d, ArH); HRMS found  $[M + 1]^+$  287.1276, C<sub>17</sub>H<sub>19</sub>O<sub>4</sub> requires  $[M + 1]^+$  287.1278; Anal. Calcd C<sub>18</sub>H<sub>20</sub>O<sub>5</sub>·0.15H<sub>2</sub>O: C, 70.65; H, 6.38. Found C, 70.56; H, 6.56.

#### 2.1.5. (E)-4-Hydroxy-3,5,4'-trimethoxystilbene (**4**)

White solid (0.10 g, 62%); TLC: *R<sub>f</sub>* 0.30 (ethyl acetate/petroleum ether 2:8); *m/z* [EI] 286 ( $[M]^+$ , 100%),  $\delta_H$  (CDCl<sub>3</sub>) 3.80 (3H, s, OMe), 3.90 (6H, s, 2 × OMe), 5.50 (1H, bs, OH), 6.70 (2H, s, ArH), 6.82 (2H, d, ArH), 6.85 (1H, d, *J* = 14 Hz, CH=CH), 6.90 (1H, d, *J* = 14 Hz, CH=CH), 7.43 (2H, d, ArH); HRMS found  $[M + 1]^+$  287.1279, C<sub>17</sub>H<sub>19</sub>O<sub>4</sub> requires  $[M + 1]^+$  287.1278; Anal. Calcd C<sub>17</sub>H<sub>18</sub>O<sub>4</sub>·0.15H<sub>2</sub>O: C, 70.65; H, 6.38. Found C, 70.68; H, 6.31.

#### 2.1.6. (E)-3-Hydroxy-4,5,4'-trimethoxystilbene (**5**)

White solid (0.07 g, 98%); m.p. 152–154 °C; TLC: *R<sub>f</sub>* = 0.35 (ethyl acetate/petroleum ether 1:1); Mass Spectrum *m/z* [EI] 287 ( $[M + 1]^+$ , 100%),  $\delta_H$  (CDCl<sub>3</sub>, 400 MHz) 3.80 (3H, s, OMe), 3.90 (6H, s, 2 × OMe), 5.70 (1H, bs, OH), 6.60 (1H, d), 6.75 (1H, d), 6.90 (4H, m), 7.40 (2H, d); <sup>13</sup>C NMR (CDCl<sub>3</sub>)  $\delta$ : 53.34, 55.92, 61.06, 102.48, 105.96, 114.19, 126.40, 127.69, 127.99, 130.12, 130.24, 133.98, 135.16, 149.42, 152.46, 159.35.

### 2.2. Effects of DMU compounds on proliferation of cancer cell lines HepG2 and MCF-7

In the present study the antitumor effects of **1** and its metabolites were investigated in cancer cell lines by means of cytotoxic MTT assays and cell cycle analysis. **1** and **2** exhibited submicromolar

toxicity in the MCF-7 breast adenocarcinoma and liver hepatoma HepG2 cancer cells, whereas **3**, **4** and **5** were inactive in terms of 50% inhibition of cellular proliferation ( $IC_{50}$ ) (Fig. 2). **1** was slightly more potent than **2** with an approximate  $IC_{50}$  of 0.3  $\mu$ M. Since **3**, **4** and **5** were considerably inactive in the MTT assay, we focused our analysis on **1** and **2**. In order to investigate which phase of the cell cycle was more profoundly affected, MCF-7 and HepG2 cells were treated with 10  $\mu$ M of **1** or **2** for 24 h, and the percentage of cells in each phase of the cell cycle was measured by flow cytometry. Both compounds induced G2/M arrest in MCF-7 and HepG2 cells with a lesser degree of G1 and S phase arrest (Fig. 3). HepG2 cells were more sensitive to both **1** and **2** treatments than MCF-7 cells. In order to examine whether **1** and **2** were more active in rapidly dividing cancer cells, their antitumor effects on HeLa uterine cervix adenocarcinoma cells were investigated. Although a 10- $\mu$ M treatment of **1** or **2** resulted in a greater degree of G2/M arrest in HeLa cells as opposed to MCF-7 or HepG2 cells, the overall cytotoxic effect, determined by the MTT assay, in the HeLa cells revealed similar  $IC_{50}$  values with those reported in the latter two cell lines (data not shown).

### 2.3. Induction of apoptosis by **1** and **2**

Initial investigations of cellular morphology using light microscopy revealed floating **2**-treated MCF-7 or HepG2 cells with condensed cellular membrane. This led us to hypothesize that **2** induces apoptosis in a similar fashion as reported previously for **1** [5]. Cell cycle analysis demonstrated that, in addition to the G2/M block, both **1** and **2** induced apoptosis of a small fraction of cells, as determined by the subG1 phase (Fig. 3A and B). This result was confirmed by DAPI staining which revealed nuclear fragmentation of MCF-7 cells after treatment with concentrations of 30  $\mu$ M of **1** or **2** for 24 h (Fig. 4A). Nuclear fragmentation using DAPI staining was not evident at lower concentrations of 10  $\mu$ M (data not shown).

### 2.4. Effect of **1** and **2** on $\beta$ -tubulin and cell cycle protein expression in MCF-7 and HepG2 cells

Based on the initial observations that treatment with **1** and **2** results in cell cycle arrest of cancerous cells in the G2/M phase and previous studies that demonstrated the antimetabolic activity of **1** [5], the expression of  $\beta$ -tubulin was investigated following treatment of MCF-7 and HepG2 cells with both compounds by Western immunoblotting and immunofluorescence staining. MCF-7 cells were treated with 0, 10 and 30  $\mu$ M of **1** or **2** for 24 and 48 h. Incubation of MCF-7 cells at concentrations of 10  $\mu$ M for 24 h had no effect on  $\beta$ -tubulin distribution, as determined by immunostaining (data not shown). Treatment of 30  $\mu$ M **1** or **2** for 24 h decreased the localization of  $\beta$ -tubulin expression around the nucleus of the MCF-7 cells (Fig. 4B). This effect was more profound at the 48 h period (Fig. 4C). In order to prove that this effect was due to the agents acting on  $\beta$ -tubulin rather than a cytotoxic effect decreasing the number of live cells, Western immunoblotting was employed to examine the protein levels of  $\beta$ -tubulin in both the MCF-7 and HepG2 cells following treatment with **1** or **2**. The compounds induced a downregulation of  $\beta$ -tubulin expression in the MCF-7 and HepG2 cells at concentrations of 30  $\mu$ M or higher (Figs. 5 and 6). Both **1** and **2** caused a dose-dependent downregulation of cyclin D1 levels, as well as an upregulation of the tumor-suppressor protein p53 (Figs. 5 and 6). **1** was somewhat more potent in inducing the aforementioned changes in both HepG2 and MCF-7 cells.

### 2.5. Molecular modeling of **1** and **2** docked at the paclitaxel binding site of $\beta$ -tubulin

The *trans*-tetramethoxystilbene analogue **1**, but not resveratrol (Fig. 1), has been recently shown to enhance tubulin polymerization *in vitro* [5]. For that reason, compounds **1** and **2** are expected to

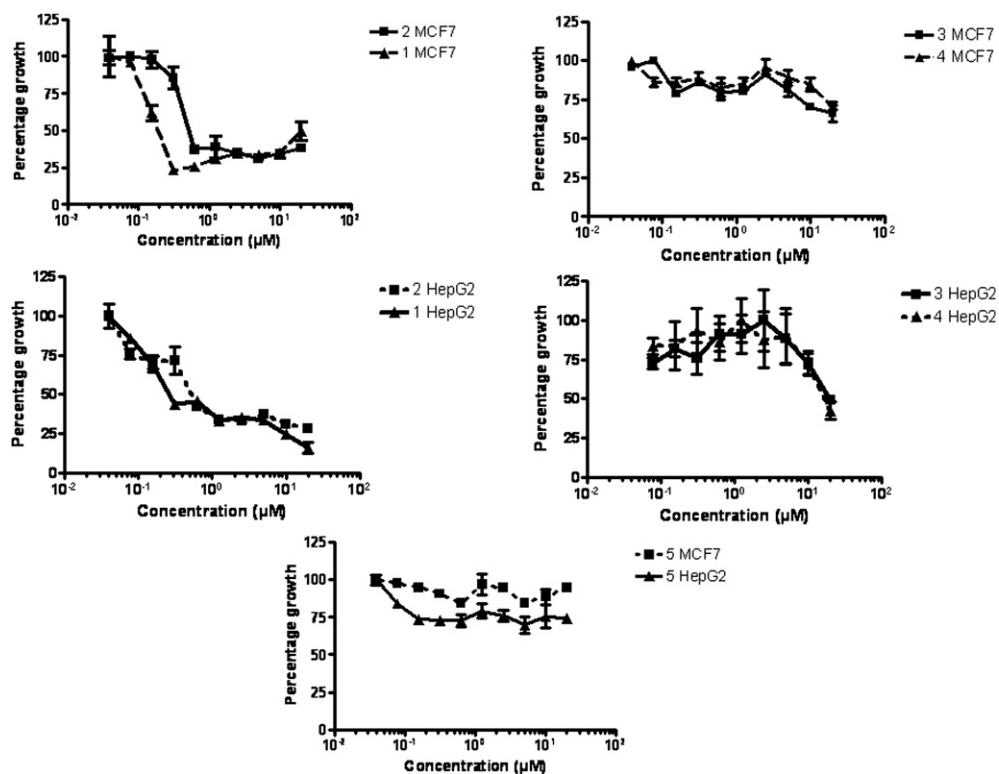
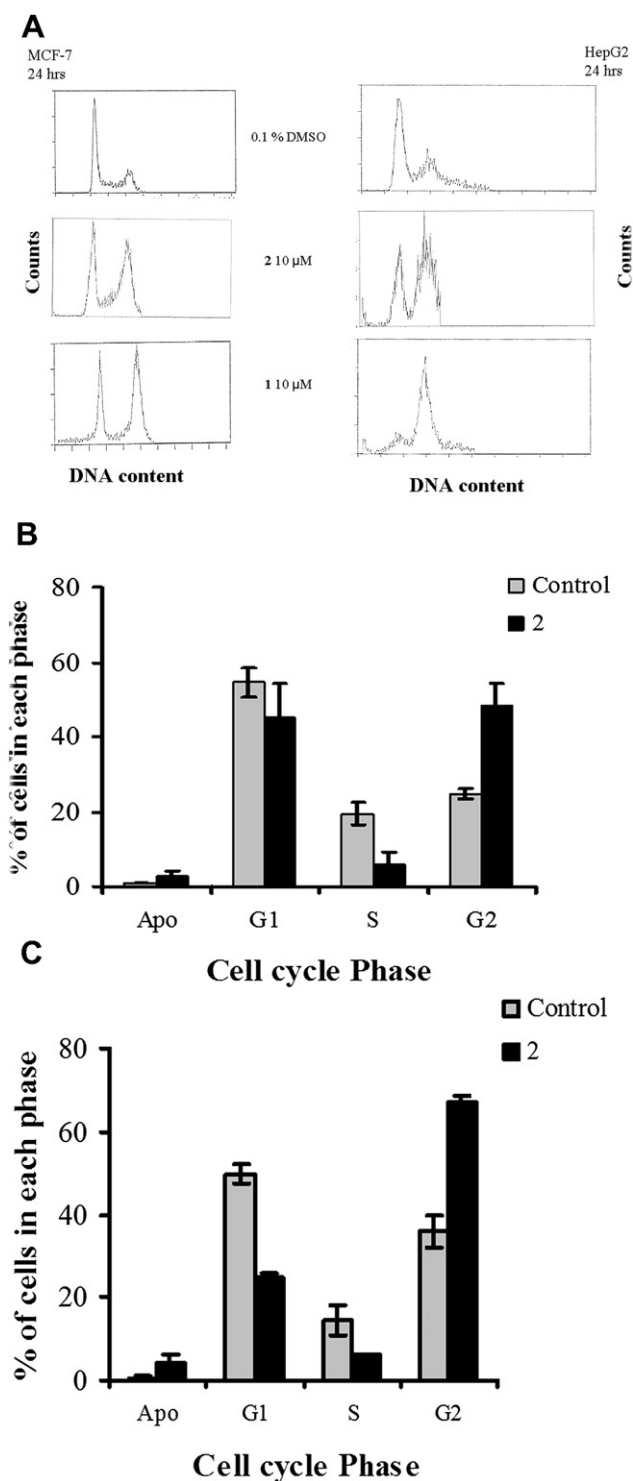
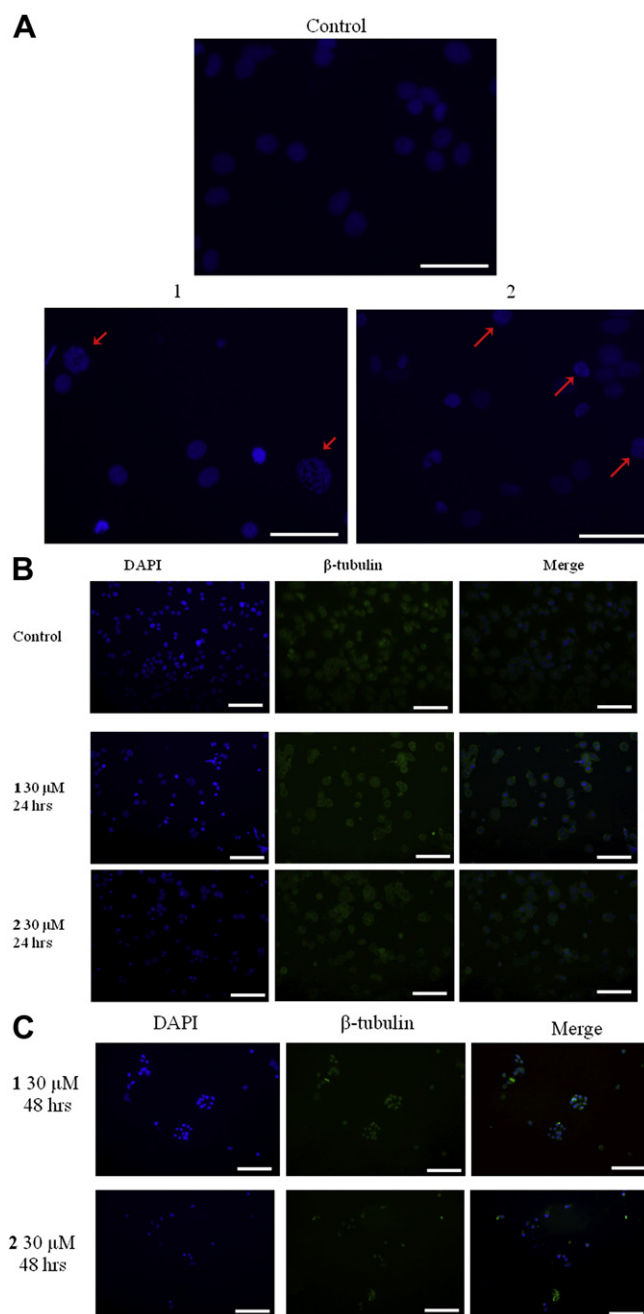


Fig. 2. The cytotoxicity of compounds **1**, **2**, **3**, **4** and **5** in MCF-7 and HepG2 cells. Compounds **1**, **2**, **3**, **4** and **5** were incubated at a concentration range covering 0.078–20  $\mu$ M for 96 h and cell viability measured using the MTT assay, as described in Experimental Protocols. Experiments were performed at least 3 times and error bars indicate S.D. of the mean.



**Fig. 3.** Cell cycle profile of HepG2 and MCF-7 cells following treatment with **1** or **2**. The cells were treated with Propidium Iodide solution in PBS (50  $\mu\text{g}/\text{mL}$ ) containing RNase A (100  $\mu\text{g}/\text{mL}$ ) and fluorescence was measured in a Beckman Coulter flow cytometer as described in *Experimental Protocols*. A) Representative DNA analysis histograms. B) Percentage of MCF-7 cells in each phase of the cell cycle measured, following 10  $\mu\text{M}$  of **2** treatment. C) Percentage of HepG2 cells in each phase of the cell cycle measured, following 10  $\mu\text{M}$  of **2** treatment. Error bars are S.D. of the mean for at least  $n=3$  determinations.

mediate tubulin polymerization through binding at the paclitaxel site of  $\beta$ -tubulin [14]. To examine the putative interaction of the *trans*-stilbene analogues with  $\beta$ -tubulin, molecular docking calculations were performed using the refined crystallographic structure



**Fig. 4.** Induction of nuclear fragmentation and  $\beta$ -tubulin sorting by **1** and **2** in MCF-7 cells. Cells were grown on coverslips, treated with compounds for 24 and 48 h and stained with  $\beta$ -tubulin primary antibody. Fluorescence was measured using a secondary anti-mouse IgG conjugated with AlexaFluor as described in *Experimental Protocols*. A) DAPI staining following 30  $\mu\text{M}$  treatment of compounds **1** and **2** for 24 h. Red arrows indicate fragmented nuclei. B) Immunostaining for  $\beta$ -tubulin at 24 h treatment and at C) 48 h treatment (Bars 10  $\mu\text{M}$ ). (For interpretation of the references to colour in this figure legend, the reader is referred to the web version of this article.)

of the  $\alpha\beta$ -tubulin dimer [15]. Compounds **1–5** and resveratrol were docked at the paclitaxel binding site of  $\beta$ -tubulin (Fig. 7A) using full conformational flexibility and the new free-energy scoring function of AutoDock4 (see *Computational methods*). All compounds were predicted to bind at the paclitaxel site with at least 3 different conformations (poses) and estimated free-energies of binding at the range of  $-4.8$  to  $-5.8$  kcal/mol, with resveratrol exhibiting the lowest values. The predicted binding energies correspond to

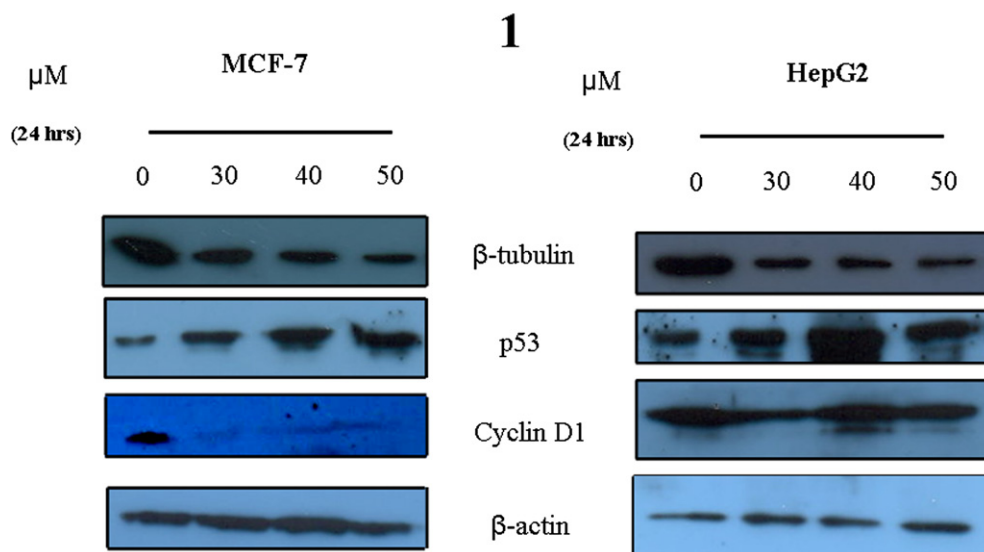


**Fig. 5.** Effects of **1** on p53, cyclin D1 and  $\beta$ -tubulin protein expression. MCF-7 and HepG2 cells were treated with **1** and western blotting carried out as described in Experimental Protocols.

inhibition constants ranging from 50 to 300  $\mu$ M, which is in agreement with the cytotoxic profile of these compounds in HepG2 and MCF-7 cells. However, given that the standard error of the scoring function is around 2.5 kcal/mol, an absolute ranking of compounds **1–5** would be highly ambiguous.

A representative pose of the active analogue **1** displays a number of contacts with critical residues at the paclitaxel site of  $\beta$ -tubulin (Fig. 7B). Specifically, the methoxy groups at ring A of **1** exhibit van der Waals contacts with residues Pro360 and Glu27, the double bond is stacked on Phe272 and ring-B exhibits a “T-shaped” aromatic interaction with His229 and hydrophobic interactions with Leu217, Leu230 and Leu275 (Fig. 7B). Interestingly, its metabolite, DMU-214 (**2**), is predicted to bind with an equal affinity that is mediated by an additional hydrogen-bonding interaction between the 3'-OH of ring-B and Thr276 residue of  $\beta$ -tubulin (Fig. 7C). At such an orientation, the torsion angle between the phenyl and ethylene groups of **2** is about 30°, in contrast to the

approximately planar orientation of the phenyl rings of **1**. Despite of the predicted interactions between compounds **1** and **2** with critical residues of the paclitaxel site of  $\beta$ -tubulin, the binding affinity for  $\beta$ -tubulin alone is not sufficient to elucidate their inhibitory potency. This was also observed in a recent study on resveratrol analogues, in which the authors suggest that many other factors, such as absorption, distribution and metabolism, must be taken under consideration to account for the cell proliferation inhibition potency [16].

#### 2.6. Effect of **2** on expression of apoptosis-related genes in MCF-7 and HepG2 cells

The apoptotic effect of **1** has been documented in a recent report [5]. Therefore, we investigated the ability of **2** only, to induce expression of the pro-apoptotic gene Bax and the anti-apoptotic gene Bcl-xL by RT-PCR. **2** induced a dose-dependent upregulation

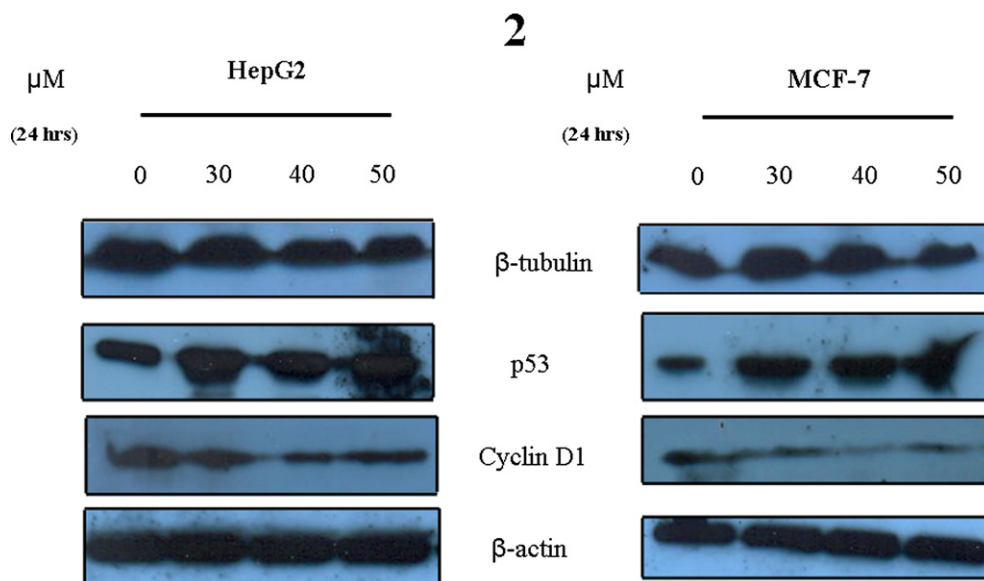


**Fig. 6.** Effects of **2** on p53, cyclin D1 and  $\beta$ -tubulin protein expression. MCF-7 and HepG2 cells were treated with DMU-214 and western blotting carried out as described in Experimental Protocols.

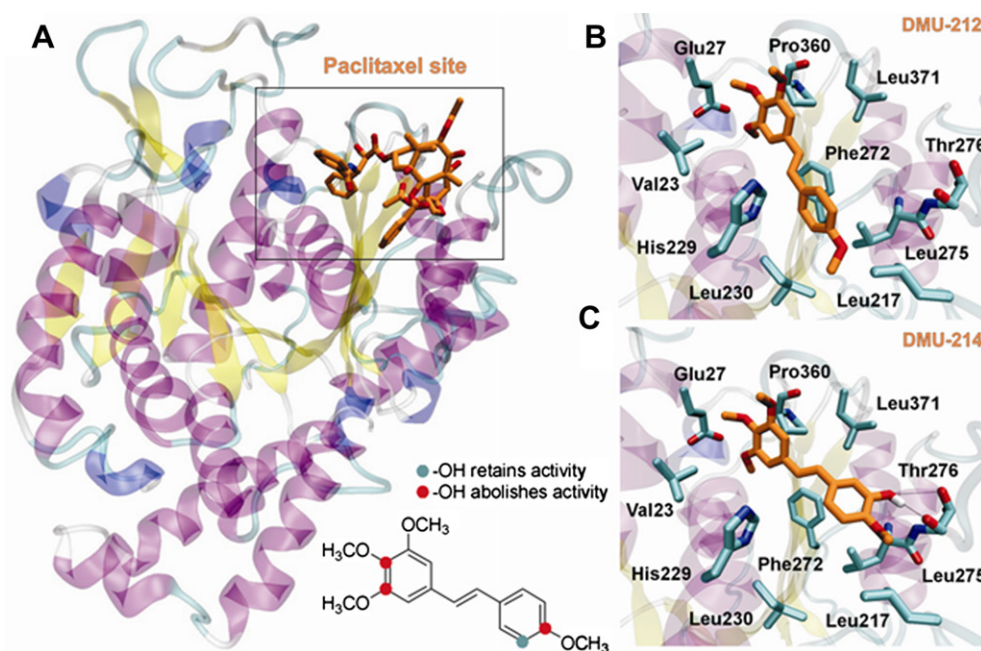


**Fig. 7.** Molecular modeling of the *trans*-stilbenes binding to  $\beta$ -tubulin. (A) Ribbon representation of  $\beta$ -tubulin with bound paclitaxel shown using orange sticks for carbon atoms, red for oxygen and blue for nitrogen. Representative poses of **1** (B) and **2** (C) docked into the paclitaxel binding site and colored according to (A). Residues of  $\beta$ -tubulin that provide contacts with the *trans*-stilbenes are shown with cyan carbons and hydrogen-bonding interactions are marked with dashed lines. Inset is also shown schematically the structural requirements for the observed antiproliferative activity of **1**. (For interpretation of the references to colour in this figure legend, the reader is referred to the web version of this article.)

of Bax mRNA levels in both MCF-7 and HepG2 cells. In contrast, a downregulation of Bcl-xL mRNA levels was noted in MCF-7 cells following **2** treatment, whereas the mRNA levels of this gene remained relatively stable in the HepG2 cells (Fig. 8A). The overall ratio of Bax/Bcl-xL mRNA levels was significantly increased in HepG2 cells following treatment of 20, 30 and 40  $\mu$ M of **2** for 24 h and in MCF-7 cells following treatment of 30 and 40  $\mu$ M (Fig. 8B).

### 3. Discussion

In the present study we evaluated the anticancer activities of (E)-3,4,5,4'-tetramethoxystilbene (**1**) and its metabolites. The most important conclusion drawn by these findings is the structure–activity relationship that is required to preserve **1** potency in inhibiting the proliferation of cancer cells. Compounds **3**, **4** and **5** differ from **1** by the presence of a hydroxyl group in place of a methoxy group. Compound **3** is the 4'-demethylated analogue of **1**, whereas **4** and **5** are the 4- and 3-demethylated analogues of **1**, respectively. Our results demonstrate that the 3,4,4'-trimethoxy substitution is necessary to retain **1** activity in inhibiting cancer cell proliferation. Hydroxylation at positions 3, 4 or 4' abolishes the activity of this compound, since **3**, **4** and **5** were inactive in terms of inhibition of cellular proliferation. This conclusion is illustrated as inset in Fig. 7.

It is generally accepted that methoxylation of flavonoids and structurally related natural compounds enhances their bioavailability and half life *in vivo* [17,18]. Walle and colleagues have demonstrated that methoxylated flavonoids show increased bioavailability due to decreased glucuronidation and phase-II conjugation reactions *in vivo* and *in vitro* [17,18]. Capping of free hydroxyl groups with methoxy groups prevents glucuronidation in liver and intestinal cells. This is one factor that has to be considered when examining the antiproliferative activity of methoxylated and hydroxylated stilbenes. Compounds that possess free hydroxyl groups may present reduced pharmacological and antiproliferative activities, due to rapid excretion.

A recent study has underlined the importance of methoxylation in *trans*-stilbenes in increasing the toxicity towards *Caenorhabditis elegans* [19]. The authors examined, amongst other compounds, resveratrol trimethyl ether, pterostilbene, (E)-3-hydroxy-5,4'-dimethoxystilbene, pinostilbene and desoxyrhapontigenin [19]. The latter compounds are based on the structure of resveratrol and possess from one to three methoxy substitutions in place of the hydroxyl groups of resveratrol. The order of potency was as follows: resveratrol trimethyl ether > (E)-3-hydroxy-5,4'-dimethoxystilbene > pterostilbene > desoxyrhapontigenin > pinostilbene. Taken collectively with our results these data indicate that for maximum toxicity methoxy substitutions on ring A and one methoxy substitution on ring-B are required. This may indicate a favored binding orientation to a putative biological target such as tubulin, or a desired pharmacodynamic index that increases the bioavailability and bio-stability of the methoxylated stilbenes.

Our findings indicate that **1** induced a decrease in  $\beta$ -tubulin expression as demonstrated by Western immunoblotting and immunofluorescence microscopy. Tubulin is composed of a heterodimer which consists of two closely related proteins  $\alpha$  and  $\beta$  tubulin. Tubulin polymerizes to form microtubules that comprise the main element for the formation of the mitotic spindle during mitosis. Anti-tubulin drugs act by interfering with tubulin assembly. There are two distinct modes by which anti-tubulin drugs act. The first class of compounds binds preferentially to polymerized tubulin and enhances its polymerization further [20]. This causes hyperassembly of microtubules and increased stability, thus altering the dynamics of the mitotic spindle. Microtubules appear shorter in length and frequently bundled compared to normal untreated mitotic cells [20]. The second class of compounds binds preferentially to the  $\alpha$ , $\beta$ -tubulin heterodimer, rather than the polymerized form of tubulin and inhibit its polymerization [20]. This inhibits the assembly of microtubules and causes their disappearance in both the interphase and mitotically arrested cells [20].

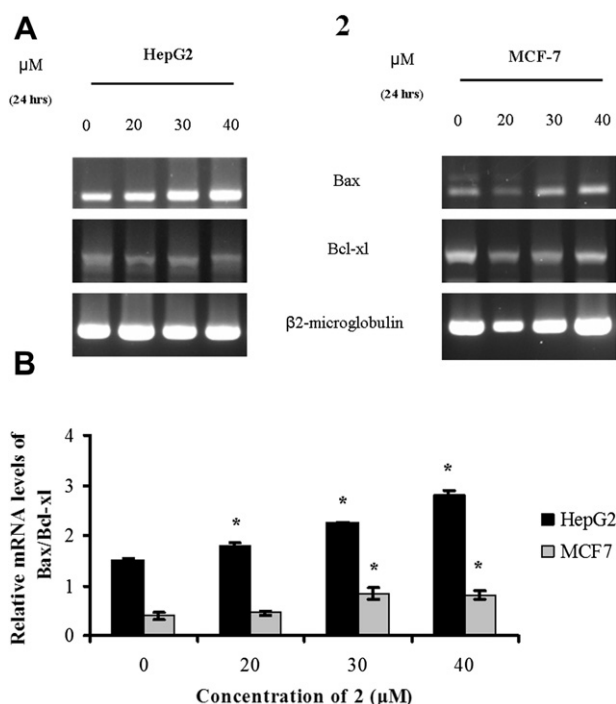


**Fig. 8.** The effect of **2** on the expression of apoptotic related genes Bax and Bcl-xL. **2** was incubated with MCF-7 or HepG2 cells for 24 h and RT-PCR carried out as described in Experimental Protocols. A) Representative trace of mRNA expression of Bax and Bcl-xL, following **2** treatment. B) Bax/Bcl-xL mRNA levels in MCF-7 and HepG2 cells. Results are expressed as means  $\pm$  S.D. for at least  $n = 3$  determinations. \*Statistically different than control  $p < 0.05$ .

Compounds that belong to the first category include paclitaxel and epothilones, whereas drugs that fall in the second class include colchicine, combretastatin A4 and the vinca alkaloids [20]. Combretastatin A4 (the *cis*-isomer of (E)-3,4,5,4'-tetramethoxystilbene, **2**) and related analogues mediate their antitumor effects by binding at the colchicine site of tubulin [21,16]. Recently, the *trans*-stilbene analogue **1**, but not resveratrol (Fig. 1), has been shown to significantly enhance tubulin polymerization *in vitro* [5]. Therefore, compounds **1** and **2** are expected to mediate tubulin polymerization through binding at the paclitaxel site of  $\beta$ -tubulin [14].

With respect to the observed antiproliferative structure–activity relationships of the *trans*-stilbene analogues studied (Fig. 7 inset) their binding affinity for  $\beta$ -tubulin alone is not sufficient to elucidate their inhibitory potency. As noted in a recent study of a series of *trans* and *cis* resveratrol analogues, many other factors such as absorption, distribution and metabolism must be taken under consideration to account for their cell proliferation inhibition potency [16]. The hydroxy-substitutions of compounds **3–5** probably renders them less lipophilic and more prone to metabolic conversion and oxidation.

Induction of apoptosis by **2** and **1** was associated with an upregulation of the cell cycle inhibitor p53. Both MCF-7 and HepG2 cells contain wild type p53 [22,23]. p53 induction is a mechanism that protects the cell in response to UV radiation or DNA damage caused by various agents from entering cell division. Apoptosis is then activated, and the cell does not proceed to the next cell division. There are two distinct pathways that lead to the induction of apoptosis. The extrinsic pathway depends on extracellular signals transduced through the death receptor complex, whereas the intrinsic pathway is promoted in response to intracellular stress from a number of factors. Induction of apoptosis involving modulation of p53 and Bax/Bcl-2 family proteins has been shown to be an important pathway that applies to several chemopreventive agents

[24–26]. We observed that **2** caused an upregulation of the pro-apoptotic gene Bax and a downregulation of the anti-apoptotic gene Bcl-xL (in MCF-7 cells). The anti-apoptotic proteins Bcl-2 and Bcl-xL are transcriptionally suppressed by p53 and along with the pro-apoptotic protein Bax control the release of cytochrome c from the mitochondria to the cytosol and the activation of caspase-3 which is one of the final-executioner proteins involved in the apoptotic pathway. The ratio of pro-apoptotic to anti-apoptotic protein levels is a critical determinant of the cell's fate to enter apoptosis. **2** increased the Bax/Bcl-xL mRNA levels in both HepG2 and MCF-7 cells, indicating that induction of apoptosis is a key event for the mechanism of antiproliferative action of this drug.

Compounds **1** and **2** induced G2/M arrest to a greater extent than apoptosis. This is a common phenomenon that has been observed previously for structurally related stilbenes [27]. Anti-cancer agents that disrupt the microtubule apparatus are associated with G2/M arrest of cancer cells followed by apoptosis [27]. Based on this evidence and the fact that the antiproliferation of **1** and **2** was attributed mainly to G2/M arrest, it is conceivable that the G2/M block and  $\beta$ -tubulin downregulation precede the induction of apoptosis, which is a secondary effect. In addition some antimitotic agents such as nocodazole, which disrupts microtubules by binding to  $\beta$ -tubulin, induce apoptosis in a p53-independent manner [28,29]. Whether **1** and **2** are capable of inducing apoptosis in the absence of p53 remains ill-defined, although the results clearly indicate that in wild type p53 cancer cell lines, the expression of this transcription factor is increased following treatment by the latter compounds.

Compound **1** was originally designed to be a cytochrome P450 activated prodrug [30]. *In vitro* and *in vivo* metabolism of this agent has revealed the conversion to the five metabolites **2**, **3**, **4**, **5** and DMU-295 [13]. The major metabolites found in plasma extracts were DMU-295 (4,4' didesmethyl **1**) and **4**, whereas in mouse liver microsomes **2** and **4** predominated [13]. Since DMU-295 occurs by two demethylation reactions, it is tempting to speculate that it will have decreased antiproliferative activity compared to **1**, as both **3** and **4**, the 4' and 4-demethylated analogues of **1**, were inactive. In addition, conversion to DMU-295 cannot proceed without conversion to either **4** or **3**. Collectively with the results by Sale and colleagues, the data demonstrates that metabolism of **1** *in vivo* leads notably to inactivation of its anticancer activity, rather than activation, since **2** was produced in small quantities in mouse plasma. In mouse liver microsomes a substantial conversion of **1** to **2** was noted along with the conversion to **4**. In combination with the results presented herein on the activity of **2** in human hepatoma HepG2 cells, the study by Sale et al. indicates that **1** could possess some therapeutic implications for liver cancer, through the conversion to **2** although further studies are required to confirm its clinical efficacy *in vivo*.

Activation or deactivation of anticancer drugs is an essential step towards their chemotherapeutic efficacy. Cytochrome P450 metabolism activates AQ4N to AQ4N-oxide, which demonstrates *in vivo* antitumor activity, whereas hydroxylation of Taxol by cytochrome P450 CYP1B1 results in loss of its anticancer activity [31,32]. Consequently the successful use of an anticancer drug in clinical trials requires extensive investigation of its *in vivo* metabolism as well as the determination of the antitumor activity of its metabolites.

In conclusion, the present study compared the antiproliferative activity of the resveratrol analogue **1** with that of its metabolites **2**, **3**, **4** and **5**. All of the metabolites with the exception of **2** were inactive in inhibiting 50% proliferation of MCF-7 and HepG2 cells, whereas **2** revealed similar potency with that of **1** via induction of apoptosis and G2/M block. Antimitotic agents that contain methoxy groups and are based on the chemical structure of resveratrol are

a widely acknowledged class of anticancer compounds. However, *in vivo* metabolism of these molecules can give rise to metabolites with distinct biological properties similar to that of their parent compound. Our study reinforces the antitumor potential of the parent compound **1** and provides more evidence on the *in vivo* anticancer activity of its metabolic products.

#### 4. Conclusion

We have synthesized the anticancer compound (E)-3,4,5,4'-tetramethoxystilbene (**1**) and its metabolites (E)-3'-hydroxy-3,4,5,4'-tetramethoxystilbene (**2**), (E)-4'-hydroxy-3,4,5-trimethoxystilbene (**3**), (E)-4-hydroxy-3,5,4'-trimethoxystilbene (**4**) and (E)-3-hydroxy-4,5,4'-trimethoxystilbene (**5**) and compared the anticancer activities by conventional biological assays. **2** exhibited similar yet somewhat lower potency compared to **1**, whereas the remaining three metabolites were considerably inactive. **2** further revealed a similar mechanism of action with that of **1** via: (i) induction of p53 and Bax/Bcl-xL upregulation and consequently induction of apoptosis, (ii) induction of G2/M arrest, and (iii)  $\beta$ -tubulin downregulation. The structural components responsible for the potency of **1** have been identified as the 4'-methoxy, the 3-methoxy and the 4-methoxy substitutions. In addition the results presented support the conclusion that the antitumor activity of **1** *in vivo* is dependent mainly on the conversion to the metabolite **2**.

#### 5. Experimental protocols

##### 5.1. Materials and chemicals

MTT, PI, tissue culture reagents and media, Western blotting lysis buffer, DTT and DAPI were from Sigma–Aldrich (Life Science Chemicals, Athens, Greece). Western blotting reagents were from Biorad (Biorad Laboratories, Athens, Greece) whereas RT-PCR reagents from Promega (SB Biotechnology Suppliers, Athens, Greece). Polyclonal antibody for cyclin D1 and monoclonal antibody for p53 were from Santa Cruz Biotechnologies (Heidelberg, Germany). Monoclonal antibodies for  $\beta$ -tubulin and  $\beta$ -actin were from Sigma–Aldrich (Life Science Chemicals, Athens, Greece). Secondary antibodies for western blotting were from Santa Cruz Biotechnologies, whereas for immunofluorescence from Invitrogen (Antisel SA, Thessaloniki, Greece). Reagents for chemistry synthesis were purchased from Sigma–Aldrich (Poole, UK) or Fisher Scientific (Loughborough, UK).

The  $^1\text{H}$  and  $^{13}\text{C}$  NMR spectra were recorded on a 400-MHz super-conducting Bruker Spectrometer (Karlsruhe, Germany) at 30 °C. Mass spectra were recorded on a Micromass Quattro II low resolution triple quadrupole mass spectrometer (EPSRC National Mass Spectrometry Service Centre, Swansea UK).

##### 5.2. Synthesis of (E)-3,4,5,4'-tetramethoxystilbene (**1**) and metabolites

###### 5.2.1. Synthesis of (E)-3,4,5,4'-tetramethoxystilbene (**1**)

A solution of *n*-butyllithium in hexanes (1.49 mL, 2.4 mmol, 1.6 M in hexane) was added dropwise to a stirred suspension of the appropriate benzyltriphenylphosphonium chloride (2.4 mmol) in anhydrous tetrahydrofuran (THF) (20 mL), at  $-20\text{ }^\circ\text{C}$ , under nitrogen. The resulting red suspension was stirred for 20 min at  $-20\text{ }^\circ\text{C}$  and then the appropriate benzaldehyde (2.4 mmol), in anhydrous THF (10 mL) was added dropwise. The reaction was stirred for 1 h at  $-20\text{ }^\circ\text{C}$  and then allowed to warm to room temperature and stirred overnight. The progress of the reaction was monitored by TLC [ $R_f = 0.69$  (ethyl acetate/petroleum ether 4:6)]. The reaction mixture was quenched with ice-water (40 mL) and

extracted with ethyl acetate ( $3 \times 20\text{ mL}$ ). The combined organic extracts were washed with water ( $2 \times 20\text{ mL}$ ), brine ( $2 \times 20\text{ mL}$ ) and dried over anhydrous magnesium sulphate. The solvent was removed *in vacuo*. Flash column chromatography (petroleum ether 40–60 with an increasing gradient of ethyl acetate (20–40%)) afforded **1** as white crystals.

###### 5.2.2. Synthesis of 3-*tert*-butyldimethylsiloxy-4-methoxybenzaldehyde (Step 1)

*tert*-Butyldimethylsilyl chloride (6 g, 39.6 mmol) was added to a stirred solution of 3-hydroxy-4-methoxybenzaldehyde (5.0 g, 33 mmol) and *N,N*-diisopropylethylamine (8.5 mL, 50 mmol) in anhydrous DMF (100 mL) under nitrogen. After 2 h the reaction was quenched with water (100 mL) and extracted with ethyl acetate ( $3 \times 100\text{ mL}$ ). The combined organic extracts were washed with saturated sodium bicarbonate ( $3 \times 50\text{ mL}$ ), brine solution ( $3 \times 50\text{ mL}$ ) and dried over anhydrous magnesium sulphate. The solvent was removed *in vacuo* to afford a colourless oil.

###### 5.2.3. Synthesis of 3-(*tert*-butyldimethylsiloxy)-4, 3',4',5'-tetramethoxystilbene (Step 2)

*n*-Butyllithium solution (5.5 mL, 14 mmol, 1.6 M in hexanes) was added dropwise to a solution of 3,4,5-trimethoxybenzyltriphenylphosphonium chloride (6 g, 13 mmol) in anhydrous THF (100 mL) at  $-20\text{ }^\circ\text{C}$  under nitrogen. The reaction was stirred for 20 min after which a solution of 3-*tert*-butyldimethylsiloxy-4-methoxybenzaldehyde (3.33 g, 10 mmol) in anhydrous THF (25 mL) was added dropwise. The reaction was allowed to warm to room temperature and stirred for 3 h. The reaction was quenched with ice-water (100 mL) and extracted with ethyl acetate ( $3 \times 50\text{ mL}$ ). The combined organic extracts were washed with brine solution ( $3 \times 50\text{ mL}$ ), dried over anhydrous magnesium sulphate and the solvent removed *in vacuo*. Flash column chromatography ( $\text{SiO}_2$ , pet:ether with an increasing gradient of ethyl acetate (0–2%)) afforded TBDMS-protected DMU-214 as a white solid.

###### 5.2.4. Synthesis of (E)-3'-Hydroxy-3,4,5,4'-tetramethoxystilbene (**2**) (Step 3)

A solution of tetrabutylammonium fluoride in THF (2.2 mL, 2.2 mmol, 1 M in THF) was added to a stirred solution of 3-(*tert*-butyldimethylsiloxy)-4,3',4',5'-tetramethoxystilbene (0.94 g, 2.2 mmoles) in THF (20 mL) at room temperature. After 40 min, the reaction was quenched with water (10 mL) and extracted with ethyl acetate ( $3 \times 5\text{ mL}$ ). The combined organic extracts were dried over anhydrous magnesium sulphate and the solvent removed *in vacuo*. Flash column chromatography ( $\text{SiO}_2$ , pet:ether (40:60) with an increasing gradient of ethyl acetate (10–30%)) afforded DMU-214 as white solid.

The above procedure was followed similarly for the synthesis of **3**, **4**, and **5**.

##### 5.3. Cell culture

MCF-7, HepG2 and HeLa cells were maintained in RPMI-1640 (MCF-7) and DMEM (HeLa and HepG2) containing 10% (v/v) heat-inactivated (56 °C for 45 min to inactivate complement) fetal calf serum at 37 °C in 5%  $\text{CO}_2$ /95% air with 100% humidity and were passaged using trypsin-EDTA. Cultured cells were routinely passaged every 3–4 days.

##### 5.4. MTT assay

MCF-7, HepG2 and HeLa cells were plated in 96-well flat bottomed plates and left to grow for 24 h. The following morning the medium was removed, and compounds **1**, **2**, **3**, **4**, **5** were added

at serial dilutions at a concentration range of 0.079–20  $\mu\text{M}$  and left for 96 h. Cell viability was measured spectrophotometrically using MTT as a substrate, as described in a previous study [33].

### 5.5. FACS analysis

MCF-7 or HepG2 cells were cultured in T75 flasks. The cells were serum starved for 24 h and then compounds **1** and **2** (10  $\mu\text{M}$ ) were added for 24 h. The cells were washed once with PBS, trypsinized and collected in a sterile Eppendorf. The pellet was washed again with PBS, to remove traces of trypsin and medium and was fixed in 70% ethanol for at least 2 h. PI was added to the cellular pellet at a concentration of 50  $\mu\text{g}/\text{mL}$  containing RNase (100  $\mu\text{g}/\text{mL}$ ). Fluorescence intensity was measured in a Beckman Coulter flow cytometer at PMT4. At least 10,000 events were acquired. Data analysis and acquisition were performed as described previously [33].

### 5.6. DAPI staining and immunofluorescence

MCF-7 cells were grown in a 24-well plate on coverslips at a density of  $8 \times 10^4$  cells/well. Compounds **1** and **2** were added to the cells at 10 and 30  $\mu\text{M}$  concentrations for 24 and 48 h. The cells were washed twice with PBS and 1 $\times$  fixation solution (Invitrogen, Thessaloniki, Greece) was added for 10 min. The fixation solution was removed and an additional washing step with PBS was performed. The cells were then incubated for 10 min with 1X permeabilisation solution (Invitrogen, Thessaloniki, Greece) and then washed twice with PBS/1%FBS. 30–50  $\mu\text{L}$  of  $\beta$ -tubulin antibody was added to the coverslips at 1:200 dilution in PBS/1%FBS and the cells were incubated for 1 h at room temperature. The cells were washed gently twice with PBS/1%FBS and 20  $\mu\text{L}$  of secondary anti-mouse IgG conjugated with AlexaFluor were added at a 1:500 dilution in PBS/1%FBS. The cells were incubated at room temperature for 1 h in dark and washed twice with PBS–1%FBS. Coverslips were transferred in clean wells and DAPI working solution (5 mg/mL) was added at 1:100 dilution for 5 min on the surface of the coverslips in PBS/1%FBS. Excess DAPI was washed off twice by PBS/1%FBS and the coverslips were placed on histology slides and stored at 4  $^\circ\text{C}$  for analysis. Fluorescence was measured using a Nikon microscope as described previously [34].

### 5.7. Western blotting

MCF-7 or HepG2 cells were plated out in 6-well plates at a density of  $3 \times 10^5$  cells/mL and incubated at 37  $^\circ\text{C}$  for 24 h in the presence of **1** or DMU-214 (0, 30, 40, 50  $\mu\text{M}$ ). The medium was removed, and the cells were lysed with 100  $\mu\text{L}$  of lysis buffer containing protease inhibitor cocktail and DL-dithiothreitol (DTT, 1 mM), sonicated on ice for 5 min and finally centrifuged at 13,000 rpm at 4  $^\circ\text{C}$  for 10 min. The protein concentration required for sample loading was estimated at 0.7 mg/mL for each sample, and the protein lysate was mixed with sample buffer at a 1:1 ratio. Samples were heated at 100  $^\circ\text{C}$  for 5 min and then loaded on an acrylamide gel at a ratio of 10% for the resolving and 5% for the stacking gel. Electrophoresis was carried out for 1 h at 120 V, and the proteins were transferred by wet blotting to a PVDF membrane. The membrane was incubated in 10% milk/0.05% TBST at room temperature for 1 h by continuous shaking and further incubation with primary antibody for  $\beta$ -tubulin, p53, cyclin D1 and  $\beta$ -actin detection, diluted in 5% milk/0.05% TBST at 4  $^\circ\text{C}$  overnight. Antibody dilutions used were 1:400, 1:200, 1:200 and 1:400 for  $\beta$ -tubulin, p53, cyclin D1 and  $\beta$ -actin, respectively. The membrane was washed three times with 0.05% TBST and incubated with the secondary antibody against HRP diluted in 5% milk/0.05% TBST at

room temperature for 1.5 h. The membrane was finally exposed to ECL reagents, and the protein profile was developed on film.

### 5.8. RT-PCR

MCF-7 and HepG2 cells were seeded in T25 flasks and treated with DMU-214 at a concentration range of 20–40  $\mu\text{M}$  for 24 h. Total RNA was extracted using Trizol. Briefly, 1 mL of Trizol reagent was added to each flask, and the resulting sample was mixed with 200  $\mu\text{L}$  of chloroform and centrifuged at 14,000 rpm for 15 min at 4  $^\circ\text{C}$ . The top layer containing the RNA was removed, mixed with an equal volume of ice-cold isopropanol and stored at –20  $^\circ\text{C}$  overnight. The next morning the samples were centrifuged at 13,000 rpm for 5 min. Following centrifugation, the supernatant was removed and the resulting pellet containing the RNA was further precipitated with the addition of 70% ice-cold ethanol and centrifuged at 7500 rpm for 10 min. The supernatant was removed, and the RNA was dissolved in 25  $\mu\text{L}$  of sterile H<sub>2</sub>O. Total RNA was checked for purity by spectrophotometry and gel electrophoresis. RNA was treated with DNase for 45 min at 43  $^\circ\text{C}$  in order to avoid any possible contamination. A negative control sample was also included in each PCR reaction to rule out any amplification of contaminating DNA. cDNA was synthesized using a Promega kit, and PCR was carried out as previously described [35]. Primer sequences for Bax, Bcl-xL and  $\beta$ 2 microglobulin were obtained from previous studies [36]. Levels of mRNA were quantified by using Scion Image software and expressed as numerical values relative to the corresponding  $\beta$ 2M signal.

### 5.9. Computational methods

The coordinates of  $\beta$ -tubulin were taken from the refined model of the  $\alpha\beta$ -tubulin dimer at 3.5  $\text{\AA}$  resolution, which was retrieved from the Protein Data Bank (PDB ID: 1JFF) [15]. The 3D coordinates of compounds **1–5** were generated from their SMILES representation using Omega2.1 with standard parameters [37]. AutoDockTools1.5.4 was employed for the preparation of  $\beta$ -tubulin and ligands with the united-atom approximation [38]. Briefly, only polar hydrogen atoms were retained and Gasteiger atomic charges were assigned to both protein and ligands. Grid maps were centered at paclitaxel and comprised  $41 \times 51 \times 41$  points of 0.375  $\text{\AA}$  spacing. Docking calculations were performed using AutoDock4.2.[39]. For each complex, 100 docking calculations were performed using the Lamarckian genetic algorithm conformational search with default parameters from Autodock3 [40]. The maximum number of energy evaluations was set to  $25 \times 10^6$  and the resulted conformations were clustered with a 2- $\text{\AA}$  tolerance. VMD 1.8.7 was used for analysis of the docking results and preparation of the figures [41]. Calculations were performed using an x86\_64 quad-core workstation running Linux kernel 2.6.29.

### 5.10. Statistical analysis

Data are presented as the mean of at least three independent measurements and were analysed by the paired *t*-test and one-way ANOVA with Dunnett's post test as indicated, using GraphPadPrism.

### Conflict of Interest

The authors declare that they don't have any conflict of interest.

### Acknowledgements

The authors are thankful to Professor Brenton and team at EPSRC National Mass spectrometry facilities for carrying out analysis of synthesized compounds. This work was funded by the

Prefecture of Heraklion, Crete, Greece, ELKE University of Crete grant N. 2590.

## Appendix A. Supplementary material

Supplementary data associated with this article can be found, in the online version, at doi:10.1016/j.ejmech.2011.03.049.

## References

- [1] K.P.L. Bhat, D. Lantvit, K. Christov, R.G. Mehta, R.C. Moon, J.M. Pezzuto, *Cancer Res.* 61 (2001) 7456–7463.
- [2] H.P. Ciolino, P.J. Daschner, G.C. Yeh, *Cancer Res.* 58 (1998) 5707–5712.
- [3] R.S. Haworth, M. Avkiran, *Biochem. Pharmacol.* 62 (2001) 218–220.
- [4] S.J. Slatter, J.L. Seiz, A.C. Cook, B.A. Stagliano, C.J. Buzas, *Biochem. Biophys. Acta* 1637 (2003) 59–69.
- [5] Z. Ma, O. Molavi, A. Haddadi, R. Lai, R.A. Gossage, A. Lavasanifar, *Cancer Chemother. Pharmacol.* 63 (2008) 27–35.
- [6] Y.J. Surh, K.S. Chun, H.H. Cha, S.S. Han, Y.S. Keum, K.K. Park, S.S. Lee, *Mutat. Res.* 480–481 (2001) 243–268.
- [7] S. Banerjee, C. Bueso-Ramos, B.B. Aggarwal, *Cancer Res.* 62 (2002) 4945–4954.
- [8] L. Tessitore, A. Davit, I. Sarotto, G. Caderni, *Carcinogenesis* 21 (2000) 1619–1622.
- [9] S. Sale, R.G. Tunstall, K.C. Ruparelia, G.A. Potter, W.P. Steward, A.J. Gescher, *Int. J. Cancer* 115 (2005) 194–201.
- [10] D.A. Goldberg, J. Yan, G.J. Soleas, *Clin. Biochem.* 36 (2003) 79–87.
- [11] P. Saiko, M. Pemberger, Z. Horvath, I. Savinc, M. Grusch, N. Handler, T. Erker, W. Jaeger, M. Fritzer-Szekeres, T. Szekeres, *Oncol. Rep.* 19 (2008) 1621–1626.
- [12] M. Belleri, D. Ribatti, S. Nicoli, F. Cotelli, L. Forti, V. Vannini, L.A. Stivala, M. Presta, *Mol. Pharmacol.* 67 (2005) 1451–1459.
- [13] S. Sale, R.D. Verschoyle, D. Boocock, D.J.L. Jones, N. Wilsher, K.C. Ruparelia, G.A. Potter, P.B. Farmer, W.P. Steward, A.J. Gescher, *Br. J. Cancer* 90 (2004) 736–744.
- [14] E. Nogales, S.G. Wolf, K.H. Downing, *Nature* 391 (1998) 199–203.
- [15] J. Lowe, H. Li, K.H. Downing, E. Nogales, *J. Mol. Biol.* 313 (2001) 1045–1057.
- [16] F. Mazue, D. Colin, J. Gobbo, M. Wegner, A. Rescifina, C. Spatafora, D. Fasseur, D. Delmas, P. Meumier, C. Tringali, N. Latruffe, *Eur. J. Med. Chem.* 45 (2010) 2972–2980.
- [17] X. Wen, T. Walle, *Drug Metab. Dispos.* 34 (2006) 1786–1792.
- [18] T. Walle, *Free Rad. Biol. Med.* 36 (2004) 829–837.
- [19] M.A. Wilson, A.M. Rimando, C.A. Wolkow, *BMC Pharmacol.* 8 (2008) 15.
- [20] E. Hamel, *Cell Biochem. Biophys.* 38 (2003) 1–21.
- [21] N.H. Nam, *Curr. Med. Chem.* 10 (2003) 1697–1722.
- [22] M. Tsai, J.A. Cook, G.V.R. Chandramouli, W. DeGraff, H. Yan, S. Zhao, C.N. Coleman, J.B. Mitchell, E.Y. Chuang, *Cancer Res.* 67 (2007) 3845–3852.
- [23] K. Boehme, Y. Dietz, P. Hewitt, S.O. Mueller, *Toxicol. Lett.* 198 (2010) 272–281.
- [24] P. Zheng, L. Chiang, C. Lin, *Life Sci.* 76 (2005) 1367–1379.
- [25] S.K. Katiyar, A.M. Roy, M.S. Baliga, *Mol. Cancer Ther.* 4 (2005) 207–216.
- [26] C. Huang, W. Ma, A. Goranson, Z. Dong, *Carcinogenesis* 20 (1999) 237–242.
- [27] H. Li, W.K.K. Wu, Z. Zheng, C.T. Che, L. Yu, Z.J. Li, Y.C. Wu, K.W. Cheng, J. Yu, C.H. Cho, M. Wang, *Biochem. Pharmacol.* 78 (2009) 1224–1232.
- [28] M. Casenghi, M. Mangiacasale, M. Tuynder, P. Caillet-Fauquet, A. Elhajouji, P. Lavia, S. Mousset, M. Kirsch-Volders, E. Cundari, *Exp. Cell Res.* 250 (1999) 339–350.
- [29] Y. Schneider, B. Fischer, D. Coelho, S. Roussi, F. Gosse, P. Bischoff, F. Raul, *Cancer Lett.* 211 (2004) 155–161.
- [30] G.A. Potter, P.C. Butler, K.C. Ruparelia, T. Ijaz, N.C. Wilsher, E. Wanogho, H.L. Tan, T.T.V. Hoang, L.A. Stanley, M.D. Burke, *Br. J. Cancer* 86 (Suppl. 1) (2002) S117.
- [31] L.H. Patterson, G.I. Murray, *Curr. Pharm. Des.* 8 (2002) 1335–1347.
- [32] M.C. McFadyen, H.C. McLeod, F.C. Jackson, W.T. Melwin, J. Doehmer, G.I. Murray, *Biochem. Pharmacol.* 62 (2001) 207–212.
- [33] V. Androutsopoulos, R.R. Arroyo, J.F. Hall, S. Surichan, G.A. Potter, *Breast Cancer Res.* 10 (2008) R39.
- [34] P. Dimitropoulou, R. Caswell, B.P. McSharry, R.F. Greaves, D.A. Spandidos, G.W. Wilkinson, G. Sourvinos, *Eur. J. Cell Biol.* 89 (2010) 758–768.
- [35] V. Androutsopoulos, N. Wilsher, R.R.J. Arroyo, G.A. Potter, *Cancer Lett.* 274 (2009) 54–60.
- [36] G. Soufla, S. Baritaki, S. Sifakis, A. Zafiroopoulos, D.A. Spandidos, *Int. J. Biol. Markers* 20 (2005) 18–27.
- [37] J. Kirchmair, G. Wolber, C. Laggner, T. Langer, *J. Chem. Inf. Model.* 46 (2006) 1848–1861.
- [38] M.F. Sanner, *J. Mol. Graph. Model.* 17 (1999) 57–61.
- [39] R. Huey, G.M. Morris, A.J. Olson, D.S. Goodsell, *J. Comput. Chem.* 28 (2007) 1145–1152.
- [40] G. Morris, D. Goodsell, R. Halliday, R. Huey, W. Hart, R. Belew, A.J. Olson, *J. Comput. Chem.* 19 (1998) 1639–1662.
- [41] W. Humphrey, A. Dalke, K. Schulten, *J. Mol. Graph* 14 (1996) 27–38.